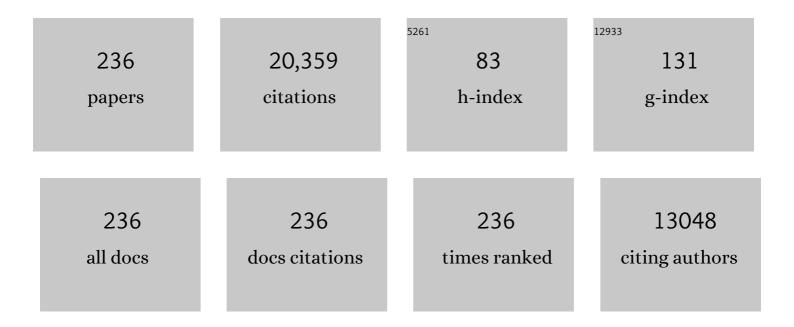
Dengsong Zhang

List of Publications by Year in descending order

Source: https://exaly.com/author-pdf/9230716/publications.pdf Version: 2024-02-01



#	Article	IF	CITATIONS
1	Selective Catalytic Reduction of NO _{<i>x</i>} with NH ₃ by Using Novel Catalysts: State of the Art and Future Prospects. Chemical Reviews, 2019, 119, 10916-10976.	23.0	1,003
2	Rational Design of High-Performance DeNO _{<i>x</i>} Catalysts Based on Mn _{<i>x</i>} Co _{3–<i>x</i>} O ₄ Nanocages Derived from Metal–Organic Frameworks. ACS Catalysis, 2014, 4, 1753-1763.	5.5	466
3	Morphology Dependence of Catalytic Properties of Ni/CeO ₂ Nanostructures for Carbon Dioxide Reforming of Methane. Journal of Physical Chemistry C, 2012, 116, 10009-10016.	1.5	453
4	Shape-controlled synthesis and catalytic application of ceria nanomaterials. Dalton Transactions, 2012, 41, 14455.	1.6	350
5	Design of graphene-coated hollow mesoporous carbon spheres as high performance electrodes for capacitive deionization. Journal of Materials Chemistry A, 2014, 2, 4739-4750.	5.2	325
6	Enhanced capacitive deionization performance of graphene/carbon nanotube composites. Journal of Materials Chemistry, 2012, 22, 14696.	6.7	318
7	Mechanistic Aspects of deNO _{<i>x</i>} Processing over TiO ₂ Supported Co–Mn Oxide Catalysts: Structure–Activity Relationships and In Situ DRIFTs Analysis. ACS Catalysis, 2015, 5, 6069-6077.	5.5	310
8	In situ supported MnOx–CeOx on carbon nanotubes for the low-temperature selective catalytic reduction of NO with NH3. Nanoscale, 2013, 5, 1127.	2.8	300
9	Three-dimensional macroporous graphene architectures as high performance electrodes for capacitive deionization. Journal of Materials Chemistry A, 2013, 1, 11778.	5.2	262
10	N, P, S co-doped hollow carbon polyhedra derived from MOF-based core–shell nanocomposites for capacitive deionization. Journal of Materials Chemistry A, 2018, 6, 15245-15252.	5.2	260
11	Synthesis of CeO2Nanorods via Ultrasonication Assisted by Polyethylene Glycol. Inorganic Chemistry, 2007, 46, 2446-2451.	1.9	244
12	Graphene-based materials for capacitive deionization. Journal of Materials Chemistry A, 2017, 5, 13907-13943.	5.2	242
13	Three-dimensional graphene-based hierarchically porous carbon composites prepared by a dual-template strategy for capacitive deionization. Journal of Materials Chemistry A, 2013, 1, 12334.	5.2	232
14	Low-temperature selective catalytic reduction of NO with NH3 over nanoflaky MnOx on carbon nanotubes in situ prepared via a chemical bath deposition route. Nanoscale, 2013, 5, 9199.	2.8	231
15	Enhanced capacitive deionization of graphene/mesoporous carbon composites. Nanoscale, 2012, 4, 5440.	2.8	230
16	Design of meso-TiO2@MnOx–CeOx/CNTs with a core–shell structure as DeNOx catalysts: promotion of activity, stability and SO2-tolerance. Nanoscale, 2013, 5, 9821.	2.8	225
17	In Situ DRIFTs Investigation of the Low-Temperature Reaction Mechanism over Mn-Doped Co ₃ O ₄ for the Selective Catalytic Reduction of NO _{<i>x</i>} with NH ₃ . Journal of Physical Chemistry C, 2015, 119, 22924-22933.	1.5	224
18	Templateâ€Free Synthesis, Controlled Conversion, and CO Oxidation Properties of CeO ₂ Nanorods, Nanotubes, Nanowires, and Nanocubes. European Journal of Inorganic Chemistry, 2008, 2008, 2429-2436.	1.0	222

#	Article	IF	CITATIONS
19	CTAB assisted hydrothermal synthesis, controlled conversion and CO oxidation properties of CeO2 nanoplates, nanotubes, and nanorods. Journal of Solid State Chemistry, 2008, 181, 1298-1306.	1.4	220
20	Immobilizing Ni nanoparticles to mesoporous silica with size and location control via a polyol-assisted route for coking- and sintering-resistant dry reforming of methane. Chemical Communications, 2014, 50, 7250-7253.	2.2	208
21	Improved NO _{<i>x</i>} Reduction in the Presence of SO ₂ by Using Fe ₂ O ₃ -Promoted Halloysite-Supported CeO ₂ –WO ₃ Catalysts. Environmental Science & Technology, 2019, 53, 938-945.	4.6	206
22	Silicon/Carbon Composite Anode Materials for Lithium-Ion Batteries. Electrochemical Energy Reviews, 2019, 2, 149-198.	13.1	205
23	Investigation of the Facet-Dependent Catalytic Performance of Fe ₂ O ₃ /CeO ₂ for the Selective Catalytic Reduction of NO with NH ₃ . Journal of Physical Chemistry C, 2016, 120, 1523-1533.	1.5	204
24	Fe ₂ O ₃ –CeO ₂ @Al ₂ O ₃ Nanoarrays on Al-Mesh as SO ₂ -Tolerant Monolith Catalysts for NO _{<i>x</i>} Reduction by NH ₃ . Environmental Science & Technology, 2019, 53, 5946-5956.	4.6	195
25	Design of multi-shell Fe ₂ O ₃ @MnO _x @CNTs for the selective catalytic reduction of NO with NH ₃ : improvement of catalytic activity and SO ₂ tolerance. Nanoscale, 2016, 8, 3588-3598.	2.8	181
26	Porous Ni–Mn oxide nanosheets in situ formed on nickel foam as 3D hierarchical monolith de-NO _x catalysts. Nanoscale, 2014, 6, 7346-7353.	2.8	178
27	Morphology-Dependent Properties of MnO _{<i>x</i>} /ZrO ₂ –CeO ₂ Nanostructures for the Selective Catalytic Reduction of NO with NH ₃ . Journal of Physical Chemistry C, 2013, 117, 10502-10511.	1.5	176
28	Grafting sulfonic and amine functional groups on 3D graphene for improved capacitive deionization. Journal of Materials Chemistry A, 2016, 4, 5303-5313.	5.2	175
29	SO ₂ -Tolerant Selective Catalytic Reduction of NO _{<i>x</i>} over Meso-TiO ₂ @Fe ₂ O ₃ @Al ₂ O ₃ Monolith Catalysts. Environmental Science & Technology, 2019, 53, 6462-6473.	4.6	171
30	Boosting Toluene Combustion by Engineering Co–O Strength in Cobalt Oxide Catalysts. Environmental Science & Technology, 2020, 54, 10342-10350.	4.6	165
31	Nitrogen-doped porous carbon derived from a bimetallic metal–organic framework as highly efficient electrodes for flow-through deionization capacitors. Journal of Materials Chemistry A, 2016, 4, 10858-10868.	5.2	164
32	Capacitive Deionization of Saline Water by Using MoS ₂ –Graphene Hybrid Electrodes with High Volumetric Adsorption Capacity. Environmental Science & Technology, 2019, 53, 12668-12676.	4.6	162
33	Cation and anion Co-doping synergy to improve structural stability of Li- and Mn-rich layered cathode materials for lithium-ion batteries. Nano Energy, 2019, 57, 157-165.	8.2	162
34	Separation and recovery of heavy metal ions and salt ions from wastewater by 3D graphene-based asymmetric electrodes via capacitive deionization. Journal of Materials Chemistry A, 2017, 5, 14748-14757.	5.2	161
35	High performance ordered mesoporous carbon/carbon nanotube composite electrodes for capacitive deionization. Journal of Materials Chemistry, 2012, 22, 6603.	6.7	159
36	Rational design and in situ fabrication of MnO ₂ @NiCo ₂ O ₄ nanowire arrays on Ni foam as high-performance monolith de-NO _x catalysts. Journal of Materials Chemistry A, 2015, 3, 11543-11553.	5.2	157

#	Article	IF	CITATIONS
37	Highly dispersed CeO ₂ on carbon nanotubes for selective catalytic reduction of NO with NH ₃ . Catalysis Science and Technology, 2013, 3, 803-811.	2.1	151
38	Promotional effects of zirconium doped CeVO 4 for the low-temperature selective catalytic reduction of NO x with NH 3. Applied Catalysis B: Environmental, 2016, 183, 269-281.	10.8	151
39	Three-dimensional hierarchical porous carbon with a bimodal pore arrangement for capacitive deionization. Journal of Materials Chemistry, 2012, 22, 23835.	6.7	149
40	Scale–Activity Relationship of MnO _{<i>x</i>} -FeO _{<i>y</i>} Nanocage Catalysts Derived from Prussian Blue Analogues for Low-Temperature NO Reduction: Experimental and DFT Studies. ACS Applied Materials & Interfaces, 2017, 9, 2581-2593.	4.0	149
41	Comparative study of 3D ordered macroporous Ce _{0.75} Zr _{0.2} M _{0.05} O _{2â^îr} (M = Fe, Cu, Mn, Co) for selective catalytic reduction of NO with NH ₃ . Catalysis Science and Technology, 2014, 4, 93-101.	2.1	146
42	Design and synthesis of NiCe@m-SiO 2 yolk-shell framework catalysts with improved coke- and sintering-resistance in dry reforming of methane. International Journal of Hydrogen Energy, 2016, 41, 2447-2456.	3.8	146
43	Facet–Activity Relationship of TiO ₂ in Fe ₂ O ₃ /TiO ₂ Nanocatalysts for Selective Catalytic Reduction of NO with NH ₃ : <i>In Situ</i> DRIFTs and DFT Studies. Journal of Physical Chemistry C, 2017, 121, 4970-4979.	1.5	144
44	Graphene prepared via a novel pyridine–thermal strategy for capacitive deionization. Journal of Materials Chemistry, 2012, 22, 23745.	6.7	142
45	Structure–Activity Relationships of NiO on CeO ₂ Nanorods for the Selective Catalytic Reduction of NO with NH ₃ : Experimental and DFT Studies. Journal of Physical Chemistry C, 2014, 118, 9612-9620.	1.5	142
46	N,P-Codoped Meso-/Microporous Carbon Derived from Biomass Materials via a Dual-Activation Strategy as High-Performance Electrodes for Deionization Capacitors. ACS Sustainable Chemistry and Engineering, 2017, 5, 5810-5819.	3.2	138
47	<i>In Situ</i> Expanding Pores of Dodecahedron-like Carbon Frameworks Derived from MOFs for Enhanced Capacitive Deionization. ACS Applied Materials & amp; Interfaces, 2017, 9, 15068-15078.	4.0	134
48	Capacitive Removal of Heavy Metal Ions from Wastewater <i>via</i> an Electro-Adsorption and Electro-Reaction Coupling Process. Environmental Science & Technology, 2021, 55, 3333-3340.	4.6	129
49	High capacity and high rate capability of nitrogen-doped porous hollow carbon spheres for capacitive deionization. Applied Surface Science, 2016, 369, 460-469.	3.1	126
50	Methane dry reforming over boron nitride interface-confined and LDHs-derived Ni catalysts. Applied Catalysis B: Environmental, 2019, 252, 86-97.	10.8	126
51	Graphene-like carbon nanosheets prepared by a Fe-catalyzed glucose-blowing method for capacitive deionization. Journal of Materials Chemistry A, 2015, 3, 5934-5941.	5.2	122
52	In Situ DRIFTs Investigation of Promotional Effects of Tungsten on MnO _{<i>x</i>} -CeO ₂ /meso-TiO ₂ Catalysts for NO _{<i>x</i>} Reduction. Journal of Physical Chemistry C, 2017, 121, 25243-25254.	1.5	122
53	Improved capacitive deionization by using 3D intercalated graphene sheet–sphere nanocomposite architectures. Environmental Science: Nano, 2018, 5, 980-991.	2.2	121
54	Carbon nanotube assisted synthesis of CeO2 nanotubes. Journal of Solid State Chemistry, 2007, 180, 654-660.	1.4	120

#	Article	IF	CITATIONS
55	N,P,S-Codoped Hierarchically Porous Carbon Spheres with Well-Balanced Gravimetric/Volumetric Capacitance for Supercapacitors. ACS Sustainable Chemistry and Engineering, 2018, 6, 5265-5272.	3.2	120
56	Nanodiamond-decorated ZnO catalysts with enhanced photocorrosion-resistance for photocatalytic degradation of gaseous toluene. Applied Catalysis B: Environmental, 2019, 257, 117880.	10.8	120
57	Capacitive deionization of saline water using sandwich-like nitrogen-doped graphene composites <i>via</i> a self-assembling strategy. Environmental Science: Nano, 2018, 5, 2722-2730.	2.2	118
58	Defect-induced efficient dry reforming of methane over two-dimensional Ni/h-boron nitride nanosheet catalysts. Applied Catalysis B: Environmental, 2018, 238, 51-60.	10.8	118
59	Facile and template-free fabrication of mesoporous 3D nanosphere-like Mn _x Co _{3â^x} O ₄ as highly effective catalysts for low temperature SCR of NO _x with NH ₃ . Journal of Materials Chemistry A, 2018, 6, 2952-2963.	5.2	116
60	Enhanced catalytic performance of V ₂ O ₅ –WO ₃ /Fe ₂ O ₃ /TiO ₂ microsp for selective catalytic reduction of NO by NH ₃ . Catalysis Science and Technology, 2013, 3, 191-199.	heres	113
61	Unraveling the effects of the coordination number of Mn over α-MnO2 catalysts for toluene oxidation. Chemical Engineering Journal, 2020, 396, 125192.	6.6	110
62	Tuning the dimensions and structures of nitrogen-doped carbon nanomaterials derived from sacrificial g-C ₃ N ₄ /metal–organic frameworks for enhanced electrocatalytic oxygen reduction. Journal of Materials Chemistry A, 2018, 6, 5752-5761.	5.2	108
63	Trace-Fe-Enhanced Capacitive Deionization of Saline Water by Boosting Electron Transfer of Electro-Adsorption Sites. Environmental Science & Technology, 2020, 54, 8411-8419.	4.6	108
64	Design of modular catalysts derived from NiMgAl-LDH@m-SiO2 with dual confinement effects for dry reforming of methane. Chemical Communications, 2013, 49, 6770.	2.2	107
65	Comparative Electroadsorption Study of Mesoporous Carbon Electrodes with Various Pore Structures. Journal of Physical Chemistry C, 2011, 115, 17068-17076.	1.5	106
66	Insights into the stable layered structure of a Li-rich cathode material for lithium-ion batteries. Journal of Materials Chemistry A, 2017, 5, 19738-19744.	5.2	105
67	In situ creating interconnected pores across 3D graphene architectures and their application as high performance electrodes for flow-through deionization capacitors. Journal of Materials Chemistry A, 2016, 4, 4908-4919.	5.2	104
68	Creating 3D Hierarchical Carbon Architectures with Micro-, Meso-, and Macropores via a Simple Self-Blowing Strategy for a Flow-through Deionization Capacitor. ACS Applied Materials & Interfaces, 2016, 8, 18027-18035.	4.0	103
69	Coke- and sintering-resistant monolithic catalysts derived from in situ supported hydrotalcite-like films on Al wires for dry reforming of methane. Nanoscale, 2013, 5, 2659.	2.8	102
70	Cu-doped CeO2 spheres: Synthesis, characterization, and catalytic activity. Catalysis Communications, 2012, 26, 164-168.	1.6	101
71	Poisoning-Resistant NO _{<i>x</i>} Reduction in the Presence of Alkaline and Heavy Metals over H-SAPO-34-Supported Ce-Promoted Cu-Based Catalysts. Environmental Science & Technology, 2020, 54, 6396-6405.	4.6	101
72	Ni nanoparticles immobilized Ce-modified mesoporous silica via a novel sublimation-deposition	3.8	100

#	Article	IF	CITATIONS
73	Combination of Experimental and Theoretical Investigations of MnO _{<i>x</i>} /Ce _{0.9} Zr _{0.1} O ₂ Nanorods for Selective Catalytic Reduction of NO with Ammonia. Journal of Physical Chemistry C, 2013, 117, 9999-10006.	1.5	99
74	Photocatalytic preparation of nanostructured MnO2-(Co3O4)/TiO2 hybrids: The formation mechanism and catalytic application in SCR deNOx reaction. Applied Catalysis B: Environmental, 2017, 203, 778-788.	10.8	96
75	Promotional effects of B-terminated defective edges of Ni/boron nitride catalysts for coking- and sintering-resistant dry reforming of methane. Applied Catalysis B: Environmental, 2020, 267, 118692.	10.8	96
76	In situ synthesis of 3D flower-like NiMnFe mixed oxides as monolith catalysts for selective catalytic reduction of NO with NH3. Chemical Communications, 2012, 48, 10645.	2.2	95
77	Preparation and modification of carbon nanotubes. Materials Letters, 2005, 59, 4044-4047.	1.3	94
78	Three-dimensional micro/mesoporous carbon composites with carbon nanotube networks for capacitive deionization. Applied Surface Science, 2013, 282, 965-973.	3.1	94
79	Unraveling the Unexpected Offset Effects of Cd and SO ₂ Deactivation over CeO ₂ -WO ₃ /TiO ₂ Catalysts for NO _{<i>x</i>} Reduction. Environmental Science & Technology, 2020, 54, 7697-7705.	4.6	91
80	A facile strategy for the fast construction of porous graphene frameworks and their enhanced electrosorption performance. Chemical Communications, 2017, 53, 7465-7468.	2.2	89
81	Hexagonal boron nitride supported mesoSiO ₂ -confined Ni catalysts for dry reforming of methane. Chemical Communications, 2017, 53, 7549-7552.	2.2	89
82	Improved NO _x reduction in the presence of alkali metals by using hollandite Mn–Ti oxide promoted Cu-SAPO-34 catalysts. Environmental Science: Nano, 2018, 5, 1408-1419.	2.2	86
83	A general strategy for the in situ decoration of porous Mn–Co bi-metal oxides on metal mesh/foam for high performance de-NO _x monolith catalysts. Nanoscale, 2017, 9, 5648-5657.	2.8	84
84	Removal of ions from saline water using N, P co-doped 3D hierarchical carbon architectures <i>via</i> capacitive deionization. Environmental Science: Nano, 2018, 5, 2337-2345.	2.2	83
85	MnOx–CeOx/CNTs pyridine-thermally prepared via a novel in situ deposition strategy for selective catalytic reduction of NO with NH3. RSC Advances, 2013, 3, 8811.	1.7	82
86	Selective catalytic oxidation of NH ₃ over noble metal-based catalysts: state of the art and future prospects. Catalysis Science and Technology, 2020, 10, 5792-5810.	2.1	82
87	NaCl adsorption in multi-walled carbon nanotubes. Materials Letters, 2005, 59, 1989-1992.	1.3	81
88	A highly reactive catalyst for CO oxidation: CeO2 nanotubes synthesized using carbon nanotubes as removable templates. Microporous and Mesoporous Materials, 2009, 117, 193-200.	2.2	81
89	Effect of nanoparticles on the performance of thermally conductive epoxy adhesives. Polymer Engineering and Science, 2010, 50, 1809-1819.	1.5	81
90	Highly dispersed V2O5/TiO2 modified with transition metals (Cu, Fe, Mn, Co) as efficient catalysts for the selective reduction of NO with NH3. Chinese Journal of Catalysis, 2015, 36, 1886-1899.	6.9	81

#	Article	IF	CITATIONS
91	Selective Capacitive Removal of Pb ²⁺ from Wastewater over Redox-Active Electrodes. Environmental Science & Technology, 2021, 55, 730-737.	4.6	81
92	Highâ€Performance Microsized Si Anodes for Lithiumâ€ion Batteries: Insights into the Polymer Configuration Conversion Mechanism. Advanced Materials, 2022, 34, e2109658.	11.1	81
93	Highly active Ce1â^'Cu O2 nanocomposite catalysts for the low temperature oxidation of CO. Applied Surface Science, 2011, 257, 7551-7559.	3.1	79
94	Self-Protected CeO ₂ –SnO ₂ @SO ₄ ^{2–} /TiO ₂ Catalysts with Extraordinary Resistance to Alkali and Heavy Metals for NO _x Reduction. Environmental Science & Technology, 2020, 54, 12752-12760.	4.6	79
95	SO ₂ -Tolerant NO _{<i>x</i>} Reduction by Marvelously Suppressing SO ₂ Adsorption over Fe _{1²} Ce _{1â^1r} VO ₄ Catalysts. Environmental Science & Technology, 2020, 54, 14066-14075.	4.6	76
96	Preparation and desalination performance of multiwall carbon nanotubes. Materials Chemistry and Physics, 2006, 97, 415-419.	2.0	74
97	Morphology-dependent performance of Zr–CeVO ₄ /TiO ₂ for selective catalytic reduction of NO with NH ₃ . Catalysis Science and Technology, 2016, 6, 5543-5553.	2.1	74
98	Design of orderly carbon coatings for SiO anodes promoted by TiO2 toward high performance lithium-ion battery. Chemical Engineering Journal, 2018, 338, 488-495.	6.6	72
99	Fe ₂ O ₃ nanoparticles anchored in situ on carbon nanotubes via an ethanol-thermal strategy for the selective catalytic reduction of NO with NH ₃ . Catalysis Science and Technology, 2015, 5, 438-446.	2.1	71
100	Promotional effect of the TiO ₂ (001) facet in the selective catalytic reduction of NO with NH ₃ : in situ DRIFTS and DFT studies. Catalysis Science and Technology, 2016, 6, 8516-8524.	2.1	71
101	Dual Promotional Effects of TiO ₂ -Decorated Acid-Treated MnO _{<i>x</i>} Octahedral Molecular Sieve Catalysts for Alkali-Resistant Reduction of NO _{<i>x</i>} . ACS Applied Materials & amp; Interfaces, 2019, 11, 11507-11517.	4.0	70
102	Alkali-Resistant NO _{<i>x</i>} Reduction over SCR Catalysts via Boosting NH ₃ Adsorption Rates by In Situ Constructing the Sacrificed Sites. Environmental Science & Technology, 2020, 54, 13314-13321.	4.6	70
103	Creating Nitrogen-Doped Hollow Multiyolk@Shell Carbon as High Performance Electrodes for Flow-Through Deionization Capacitors. ACS Sustainable Chemistry and Engineering, 2017, 5, 3329-3338.	3.2	69
104	Selective Capacitive Removal of Heavy Metal Ions from Wastewater over Lewis Base Sites of S-Doped Fe–N–C Cathodes <i>via</i> an Electro-Adsorption Process. Environmental Science & Technology, 2021, 55, 7665-7673.	4.6	68
105	High Salt Removal Capacity of Metal–Organic Gel Derived Porous Carbon for Capacitive Deionization. ACS Sustainable Chemistry and Engineering, 2017, 5, 11637-11644.	3.2	67
106	Coke-resistant defect-confined Ni-based nanosheet-like catalysts derived from halloysites for CO ₂ reforming of methane. Nanoscale, 2018, 10, 10528-10537.	2.8	67
107	A MnN4 moiety embedded graphene as a magnetic gas sensor for CO detection: A first principle study. Applied Surface Science, 2019, 473, 820-827.	3.1	67
108	Confining Redox Electrolytes in Functionalized Porous Carbon with Improved Energy Density for Supercapacitors. ACS Applied Materials & Interfaces, 2018, 10, 42494-42502.	4.0	66

#	ARTICLE	IF	CITATIONS
109	Promotional effects of Fe on manganese oxide octahedral molecular sieves for alkali-resistant catalytic reduction of NOx: XAFS and in situ DRIFTs study. Chemical Engineering Journal, 2020, 381, 122764.	6.6	66
110	Alkali and Phosphorus Resistant Zeolite-like Catalysts for NO _{<i>x</i>} Reduction by NH ₃ . Environmental Science & Technology, 2020, 54, 9132-9141.	4.6	66
111	Removal of NaCl from saltwater solutions using micro/mesoporous carbon sheets derived from watermelon peel via deionization capacitors. RSC Advances, 2017, 7, 4297-4305.	1.7	64
112	Deep insight into the structure–activity relationship of Nb modified SnO ₂ –CeO ₂ catalysts for low-temperature selective catalytic reduction of NO by NH ₃ . Catalysis Science and Technology, 2017, 7, 502-514.	2.1	63
113	Efficient removal of metal ions by capacitive deionization with straw waste derived graphitic porous carbon nanosheets. Environmental Science: Nano, 2020, 7, 317-326.	2.2	63
114	Delocalization Effect Promoted the Indoor Air Purification via Directly Unlocking the Ring-Opening Pathway of Toluene. Environmental Science & Technology, 2020, 54, 9693-9701.	4.6	63
115	Enhanced capacitive deionization of saline water using N-doped rod-like porous carbon derived from dual-ligand metal–organic frameworks. Environmental Science: Nano, 2020, 7, 926-937.	2.2	63
116	High-Performance Binary Mo–Ni Catalysts for Efficient Carbon Removal during Carbon Dioxide Reforming of Methane. ACS Catalysis, 2021, 11, 12087-12095.	5.5	61
117	Cooperatively enhanced coking resistance via boron nitride coating over Ni-based catalysts for dry reforming of methane. Applied Catalysis B: Environmental, 2022, 302, 120859.	10.8	61
118	Creating graphene-like carbon layers on SiO anodes via a layer-by-layer strategy for lithium-ion battery. Chemical Engineering Journal, 2018, 347, 273-279.	6.6	60
119	NaCl adsorption in multi-walled carbon nanotube/active carbon combination electrode. Chemical Engineering Science, 2006, 61, 428-433.	1.9	59
120	Creating Sandwich-like Ti ₃ C ₂ /TiO ₂ /rGO as Anode Materials with High Energy and Power Density for Li-Ion Hybrid Capacitors. ACS Sustainable Chemistry and Engineering, 2019, 7, 15394-15403.	3.2	57
121	Capacitive deionization of saline water using graphene nanosphere decorated N-doped layered mesoporous carbon frameworks. Environmental Science: Nano, 2019, 6, 3442-3453.	2.2	55
122	Coralloid-like Nanostructured c-nSi/SiO _{<i>x</i>} @C _{<i>y</i>} Anodes for High Performance Lithium Ion Battery. ACS Applied Materials & Interfaces, 2017, 9, 28464-28472.	4.0	54
123	Capacitive Removal of Fluoride Ions via Creating Multiple Capture Sites in a Modulatory Heterostructure. Environmental Science & Technology, 2021, 55, 11979-11986.	4.6	54
124	In situ DRIFTs investigation of the reaction mechanism over MnOx-MOy/Ce0.75Zr0.25O2 (M = Fe, Co, Ni,) Tj ET	QqQ <u>9</u> 0 rg	BT /Qverlock
	SO2 tolorant NOv reduction over caria based catalysts: Shielding affects of bellandite Mn Ti evides		

Alkali-Resistant Catalytic Reduction of NO_{<i>x</i>} by Using Ceâ€"Oâ€"B Alkali-Capture Sites.
Environmental Science & amp; Technology, 2021, 55, 11970-11978.

Chemical Engineering Journal, 2020, 397, 125535.

#	Article	IF	CITATIONS
127	Synthesis and strong red photoluminescence of europium oxide nanotubes and nanowires using carbon nanotubes as templates. Acta Materialia, 2008, 56, 955-967.	3.8	48
128	Facile synthesis, characterization and low-temperature catalytic performance of Au/CeO2 nanorods. Materials Letters, 2009, 63, 2132-2135.	1.3	48
129	SO ₂ -Tolerant Catalytic Reduction of NO _{<i>x</i>} via Tailoring Electron Transfer between Surface Iron Sulfate and Subsurface Ceria. Environmental Science & Technology, 2022, 56, 5840-5848.	4.6	48
130	Influence of diameter of carbon nanotubes mounted in flow-through capacitors on removal of NaCl from salt water. Journal of Materials Science, 2007, 42, 2471-2475.	1.7	47
131	SO ₂ -Induced Alkali Resistance of FeVO ₄ /TiO ₂ Catalysts for NO <i>_x</i> Reduction. Environmental Science & Technology, 2022, 56, 605-613.	4.6	47
132	Pyridine-thermal synthesis and high catalytic activity of CeO2/CuO/CNT nanocomposites. Applied Surface Science, 2010, 256, 6795-6800.	3.1	45
133	Precise Al2O3 Coating on LiNi0.5Co0.2Mn0.3O2 by Atomic Layer Deposition Restrains the Shuttle Effect of Transition Metals in Li-Ion Capacitors. Chemical Engineering Journal, 2020, 401, 126138.	6.6	45
134	SO ₂ - and H ₂ O-Tolerant Catalytic Reduction of NO _{<i>x</i>} at a Low Temperature via Engineering Polymeric VO _{<i>x</i>} Species by CeO ₂ . Environmental Science & Technology, 2022, 56, 5170-5178.	4.6	45
135	Metal–Porphyrin: A Potential Catalyst for Direct Decomposition of N ₂ O by Theoretical Reaction Mechanism Investigation. Environmental Science & Technology, 2014, 48, 7101-7110.	4.6	44
136	Promotional effects of rare earth elements (Sc, Y, Ce, and Pr) on NiMgAl catalysts for dry reforming of methane. RSC Advances, 2016, 6, 112215-112225.	1.7	44
137	Ceria nanospindles: Template-free solvothermal synthesis and shape-dependent catalytic activity. Applied Surface Science, 2011, 257, 10161-10167.	3.1	42
138	Self-plied and twist-stable carbon nanotube yarn artificial muscles driven by organic solvent adsorption. Nanoscale, 2018, 10, 8180-8186.	2.8	42
139	Large-scale growth of hierarchical transition-metal vanadate nanosheets on metal meshes as monolith catalysts for De-NO _x reaction. Nanoscale, 2015, 7, 2743-2749.	2.8	41
140	Large-Scale and Low-Cost Motivation of Nitrogen-Doped Commercial Activated Carbon for High-Energy-Density Supercapacitor. ACS Applied Energy Materials, 2019, 2, 4234-4243.	2.5	41
141	Synergistic Catalytic Elimination of NO <i>_x</i> and Chlorinated Organics: Cooperation of Acid Sites. Environmental Science & Technology, 2022, 56, 3719-3728.	4.6	41
142	Morphology, toughness mechanism, and thermal properties of hyperbranched epoxy modified diglycidyl ether of bisphenol A (DGEBA) interpenetrating polymer networks. Polymers for Advanced Technologies, 2008, 19, 1597-1607.	1.6	40
143	Uniform ceria nanospheres: Solvothermal synthesis, formation mechanism, size-control and catalytic activity. Powder Technology, 2011, 207, 35-41.	2.1	40
144	Improved NO _{<i>x</i>} Reduction over Phosphate-Modified Fe ₂ O ₃ /TiO ₂ Catalysts <i>Via</i> Tailoring Reaction Paths by <i>In Situ</i> Creating Alkali-Poisoning Sites. Environmental Science & Technology, 2021, 55, 9276-9284.	4.6	40

#	Article	IF	CITATIONS
145	Low-Temperature Combustion of Toluene over Cu-Doped SmMn ₂ O ₅ Mullite Catalysts via Creating Highly Active Cu ²⁺ –O–Mn ⁴⁺ Sites. Environmental Science & Technology, 2022, 56, 10433-10441.	4.6	40
146	Investigations on the Antimony Promotional Effect on CeO ₂ –WO ₃ /TiO ₂ for Selective Catalytic Reduction of NO _{<i>x</i>} with NH ₃ . ChemCatChem, 2016, 8, 2267-2278.	1.8	39
147	Ultralow-Temperature NO <i>_x</i> Reduction over SmMn ₂ O ₅ Mullite Catalysts Via Modulating the Superficial Dual-Functional Active Sites. ACS Catalysis, 2022, 12, 7622-7632.	5.5	39
148	Rational design of 3D hierarchical foam-like Fe ₂ O ₃ @CuO _x monolith catalysts for selective catalytic reduction of NO with NH ₃ . RSC Advances, 2015, 5, 11013-11022.	1.7	38
149	In situ preparation of Ni nanoparticles in cerium-modified silica aerogels for coking- and sintering-resistant dry reforming of methane. New Journal of Chemistry, 2017, 41, 4869-4878.	1.4	38
150	Ultrasonic-assisted preparation of carbon nanotube/cerium oxide composites. Carbon, 2006, 44, 2853-2855.	5.4	37
151	One-pot self-assembly of multifunctional mesoporous nanoprobes with magnetic nanoparticles and hydrophobic upconversion nanocrystals. Journal of Materials Chemistry, 2011, 21, 17615.	6.7	37
152	Coking-resistant dry reforming of methane over BN–nanoceria interface-confined Ni catalysts. Catalysis Science and Technology, 2020, 10, 4237-4244.	2.1	37
153	Volume expansion restriction effects of thick TiO2/C hybrid coatings on micro-sized SiOx anode materials. Chemical Engineering Journal, 2020, 387, 124106.	6.6	37
154	<i>In situ</i> decorated MOF-derived Mn–Fe oxides on Fe mesh as novel monolithic catalysts for NO _x reduction. New Journal of Chemistry, 2020, 44, 2357-2366.	1.4	36
155	Reflux synthesis, formation mechanism, and photoluminescence performance of monodisperse Y2O3:Eu3+ nanospheres. Materials Chemistry and Physics, 2009, 117, 234-243.	2.0	35
156	Hydrothermal growth and characterization of length tunable porous iron vanadate one-dimensional nanostructures. CrystEngComm, 2014, 16, 5128-5133.	1.3	35
157	Efficient NO _{<i>x</i>} Abatement over Alkali-Resistant Catalysts via Constructing Durable Dimeric VO _{<i>x</i>} Species. Environmental Science & Technology, 2022, 56, 2647-2655.	4.6	35
158	Self-Defense Effects of Ti-Modified Attapulgite for Alkali-Resistant NO _{<i>x</i>} Catalytic Reduction. Environmental Science & Technology, 2022, 56, 4386-4395.	4.6	35
159	Boosting the Alkali/Heavy Metal Poisoning Resistance for NO Removal by Using Iron-Titanium Pillared Montmorillonite Catalysts. Journal of Hazardous Materials, 2020, 399, 122947.	6.5	34
160	Coking-resistant dry reforming of methane over Ni/γ-Al2O3 catalysts by rationally steering metal-support interaction. IScience, 2021, 24, 102747.	1.9	34
161	Removal of NaCl from saltwater solution using carbon nanotubes/activated carbon composite electrode. Materials Letters, 2006, 60, 360-363.	1.3	33
162	Sc promoted and aerogel confined Ni catalysts for coking-resistant dry reforming of methane. RSC Advances, 2017, 7, 4735-4745.	1.7	33

#	Article	IF	CITATIONS
163	Influence of carbonization of hot-pressed carbon nanotube electrodes on removal of NaCl from saltwater solution. Materials Chemistry and Physics, 2006, 96, 140-144.	2.0	32
164	Novel transparent ternary nanocomposite films of trialkoxysilane-capped poly(methyl) Tj ETQq0 0 0 rgBT /Over 110, 463-470.	lock 10 Tf 2.0	50 707 Td (me 32
165	Alkali-Resistant Catalytic Reduction of NO <i>_x</i> via Naturally Coupling Active and Poisoning Sites. Environmental Science & Technology, 2021, 55, 11255-11264.	4.6	32
166	Study of enzyme biosensor based on carbon nanotubes modified electrode for detection of pesticides residue. Chinese Chemical Letters, 2008, 19, 592-594.	4.8	31
167	Carbon nanotube-assisted synthesis and high catalytic activity of CeO2 hollow nanobeads. Materials Chemistry and Physics, 2009, 113, 527-530.	2.0	31
168	Accelerating the decomposition of KMnO ₄ by photolysis and auto-catalysis: a green approach to synthesize a layered birnessite-type MnO ₂ assembled hierarchical nanostructure. RSC Advances, 2016, 6, 14192-14198.	1.7	31
169	Alkali and Heavy Metal Copoisoning Resistant Catalytic Reduction of NO _{<i>x</i>} via Liberating Lewis Acid Sites. Environmental Science & Technology, 2022, 56, 5141-5149.	4.6	31
170	NO <i>_x</i> Reduction over Smart Catalysts with Self-Created Targeted Antipoisoning Sites. Environmental Science & Technology, 2022, 56, 6668-6677.	4.6	31
171	Ion-selective asymmetric carbon electrodes for enhanced capacitive deionization. RSC Advances, 2018, 8, 2490-2497.	1.7	30
172	Turning on electrocatalytic oxygen reduction by creating robust Fe–N _x species in hollow carbon frameworks <i>via in situ</i> growth of Fe doped ZIFs on g-C ₃ N ₄ . Nanoscale, 2020, 12, 5601-5611.	2.8	29
173	Preparation and CO conversion activity of ceria nanotubes by carbon nanotubes templating method. Journal of Rare Earths, 2008, 26, 153-157.	2.5	28
174	The complete reaction mechanism of H ₂ S desulfurization on an anatase TiO ₂ (001) surface: a density functional theory investigation. Catalysis Science and Technology, 2017, 7, 356-365.	2.1	28
175	Efficient Capacitive Deionization of Saline Water by an Integrated Tin disulfide Nanosheet@Graphite Paper Electrode via an in Situ Growth Strategy. ACS Sustainable Chemistry and Engineering, 2020, 8, 1268-1275.	3.2	28
176	Confined Catalysts Application in Environmental Catalysis: Current Research Progress and Future Prospects. ChemCatChem, 2021, 13, 2313-2336.	1.8	28
177	Unraveling the Promotion Effects of Dynamically Constructed CuO _{<i>x</i>} -OH Interfacial Sites in the Selective Catalytic Oxidation of Ammonia. ACS Catalysis, 2022, 12, 3955-3964.	5.5	28
178	Ethylene glycol reflux synthesis of carbon nanotube/ceria core–shell nanowires. Applied Surface Science, 2009, 255, 5789-5794.	3.1	27
179	Creating hierarchically macro-/mesoporous Sn/CeO ₂ for the selective catalytic reduction of NO with NH ₃ . RSC Advances, 2016, 6, 78727-78736.	1.7	27
180	Solventâ€Tunable Microstructures of Aligned Carbon Nanotube Films. Advanced Materials Interfaces, 2016, 3, 1600352.	1.9	27

#	Article	IF	CITATIONS
181	Tailored Alkali Resistance of DeNOx Catalysts by Improving Redox Properties and Activating Adsorbed Reactive Species. IScience, 2020, 23, 101173.	1.9	27
182	Beneficial synergy of adsorption–intercalation–conversion mechanisms in Nb ₂ O ₅ @nitrogen-doped carbon frameworks for promoted removal of metal ions <i>via</i> hybrid capacitive deionization. Environmental Science: Nano, 2021, 8, 122-130.	2.2	27
183	Low-temperature NOx reduction over hydrothermally stable SCR catalysts by engineering low-coordinated Mn active sites. Chemical Engineering Journal, 2022, 442, 136182.	6.6	27
184	Controllable synthesis and highly efficient electrocatalytic oxidation performance of SnO2/CNT core-shell structures. Applied Surface Science, 2009, 255, 4907-4912.	3.1	26
185	Facile synthesis, characterization, formation mechanism and photoluminescence property of Eu2O3 nanorods. Journal of Alloys and Compounds, 2009, 487, 483-488.	2.8	25
186	Template-free synthesis, characterization, growth mechanism and photoluminescence property of Eu(OH)3 and Eu2O3 nanospindles. Journal of Alloys and Compounds, 2010, 506, 446-455.	2.8	25
187	Operando Fourier Transform Infrared Investigation of Cathode Electrolyte Interphase Dynamic Reversible Evolution on Li1.2Ni0.2Mn0.6O2. ACS Applied Materials & Interfaces, 2019, 11, 45108-45117.	4.0	25
188	Sandwich-Like C@SnS@TiO ₂ Anodes with High Power and Long Cycle for Li-Ion Storage. ACS Applied Materials & Interfaces, 2020, 12, 5857-5865.	4.0	25
189	Promoting toluene oxidation by engineering octahedral units <i>via</i> oriented insertion of Cu ions in the tetrahedral sites of MnCo spinel oxide catalysts. Chemical Communications, 2020, 56, 6539-6542.	2.2	25
190	Unraveling SO2-tolerant mechanism over Fe2(SO4)3/TiO2 catalysts for NO reduction. Journal of Environmental Sciences, 2022, 111, 340-350.	3.2	25
191	Facile synthesis of ceria rhombic microplates. Journal of Materials Science, 2008, 43, 5647-5650.	1.7	24
192	Efficient catalytic combustion of toluene at low temperature by tailoring surficial PtO and interfacial Pt-Al(OH)x species. IScience, 2021, 24, 102689.	1.9	24
193	Mechanistic insight into the selective catalytic reduction of NO by NH ₃ over low-valent titanium-porphyrin: a DFT study. Catalysis Science and Technology, 2016, 6, 3878-3885.	2.1	23
194	Rapid synthesis of self-supported three-dimensional bubble-like graphene frameworks as high-performance electrodes for supercapacitors. Sustainable Energy and Fuels, 2017, 1, 1557-1567.	2.5	22
195	SO2-tolerant NOx reduction over SO42coordinated Cu-SAPO-34 catalysts via protecting the reduction and re-oxidation of Cu sites. Chemical Engineering Journal, 2022, 448, 137720.	6.6	22
196	Ionic liquid-assisted synthesis and photoluminescence property of mesoporous EuF3 nanospheres. Microporous and Mesoporous Materials, 2011, 141, 110-118.	2.2	21
197	Shape and size effects of ceria nanoparticles on the impact strength of ceria/epoxy resin composites. Particuology, 2011, 9, 80-85.	2.0	21
198	Synergistic effect of nanobarite and carbon black fillers in natural rubber matrix. Materials & Design, 2012. 35. 847-853.	5.1	21

#	Article	IF	CITATIONS
199	Light driven fabrication of highly dispersed Mn-Co/RGO and the synergistic effect in catalytic degradation of methylene blue. Materials and Design, 2018, 140, 286-294.	3.3	21
200	Fe-, N-Embedded Hierarchically Porous Carbon Architectures Derived from FeTe-Trapped Zeolitic Imidazolate Frameworks as Efficient Oxygen Reduction Electrocatalysts. ACS Sustainable Chemistry and Engineering, 2019, 7, 19268-19276.	3.2	21
201	Solvothermal synthesis of necklace-like carbon nanotube/ceria composites. Materials Letters, 2008, 62, 3821-3823.	1.3	20
202	Rapid construction of 3D foam-like carbon nanoarchitectures via a simple photochemical strategy for capacitive deionization. RSC Advances, 2017, 7, 39372-39382.	1.7	20
203	In situ imaging analysis of the inhibition effect of functional coating on the volume expansion of silicon anodes. Chemical Engineering Journal, 2021, 417, 128122.	6.6	20
204	Fast preparation of ultrafine monolayered transition-metal dichalcogenide quantum dots using electrochemical shock for explosive detection. Chemical Communications, 2016, 52, 11442-11445.	2.2	19
205	Interconnected surface-vacancy-rich PtFe nanowires for efficient oxygen reduction. Journal of Materials Chemistry A, 2021, 9, 12845-12852.	5.2	18
206	A NaNi _{0.5} Mn _{0.5} Sn _x O ₂ cathode with anti-structural deformation enhancing long lifespan and super power for a sodium ion battery. Chemical Communications, 2020, 56, 8079-8082.	2.2	17
207	Sintering- and coking-resistant nickel catalysts embedded in boron nitride supported nickel aluminate spinels for dry reforming of methane. Applied Catalysis A: General, 2022, 642, 118706.	2.2	17
208	Surfactant-assisted reflux synthesis, characterization and formation mechanism of carbon nanotube/europium hydroxide core–shell nanowires. Applied Surface Science, 2009, 255, 8270-8275.	3.1	16
209	Rapid Synthesis of Sub-5 nm Sized Cubic Boron Nitride Nanocrystals with High-Piezoelectric Behavior via Electrochemical Shock. Nano Letters, 2017, 17, 355-361.	4.5	16
210	Enhanced water purification <i>via</i> redox interfaces created by an atomic layer deposition strategy. Environmental Science: Nano, 2021, 8, 950-959.	2.2	16
211	Tuning Til̃ +-VoÂPtl̃ + interfaces over Pt/TiO2 catalysts for efficient photocatalytic oxidation of toluene. Chemical Engineering Journal, 2022, 431, 134209.	6.6	16
212	Mn–Fe bi-metal oxides in situ created on metal wire mesh as monolith catalysts for selective catalytic reduction of NO with NH ₃ . RSC Advances, 2017, 7, 40444-40451.	1.7	15
213	Oxotitanium-porphyrin for selective catalytic reduction of NO by NH ₃ : a theoretical mechanism study. New Journal of Chemistry, 2018, 42, 16806-16813.	1.4	14
214	Coking- and Sintering-Resistant Ni Nanocatalysts Confined by Active BN Edges for Methane Dry Reforming. ACS Applied Materials & Interfaces, 2022, 14, 25439-25447.	4.0	14
215	Palygorskite-cerium oxide filled rubber nanocomposites. Applied Clay Science, 2012, 67-68, 44-49.	2.6	12
216	Investigating the role of dissolved inorganic and organic carbon in fluoride removal by membrane capacitive deionization. Desalination, 2022, 528, 115618.	4.0	12

#	Article	IF	CITATIONS
217	Synergistic Ag(I)/ Bu4NBr-catalyzed fixation of CO2 to $\hat{1}^2$ -oxopropyl carbonates via propargylic alcohols and monohydric alcohols. Tetrahedron, 2019, 75, 2343-2349.	1.0	11
218	In situ growth of silicon carbide interface enhances the long life and high power of the mulberry-like Si-based anode for lithium-ion batteries. Journal of Energy Storage, 2020, 32, 101856.	3.9	11
219	Unraveling the promotional effects of NiCo catalysts over defective boron nitride nanosheets in dry reforming of methane. Catalysis Today, 2022, 402, 283-291.	2.2	11
220	Porous nanopeapod Pd catalyst with excellent stability and efficiency. Chemical Communications, 2017, 53, 740-742.	2.2	10
221	High Tap Density Li ₄ Ti ₅ O ₁₂ Anode Materials Synthesized for High Rate Performance Lithium Ion Batteries. ChemistrySelect, 2018, 3, 348-353.	0.7	9
222	Incorporation of CO ₂ into carbonates through carboxylation/hydration reaction. , 2018, 8, 803-838.		9
223	Integrated Structure of Tin-Based Anodes Enhancing High Power Density and Long Cycle Life for Lithium Ion Batteries. ACS Applied Energy Materials, 2020, 3, 9337-9347.	2.5	9
224	Photodegrading hexaazapentacene dispersant for surface-clean semiconducting single-walled carbon nanotubes. Carbon, 2016, 105, 448-453.	5.4	8
225	In situ fabrication of porous MnCo _x O _y nanocubes on Ti mesh as high performance monolith de-NO _x catalysts. RSC Advances, 2017, 7, 36319-36325.	1.7	8
226	Straightforward Design for Phenoxy-Imine Catalytic Activity in Ethylene Polymerization: Theoretical Prediction. Catalysts, 2018, 8, 422.	1.6	8
227	SO ₂ -Tolerant catalytic reduction of NO _{<i>x</i>} by confining active species in TiO ₂ nanotubes. Environmental Science: Nano, 2022, 9, 2121-2133.	2.2	8
228	Theoretical guidance and experimental confirmation on catalytic tendency of M-CeO ₂ (M) Tj ETQq(0.0.gBT	/Oyerlock 10
229	Promoting Dry Reforming of Methane Catalysed by Atomicallyâ€Dispersed Ni over Ceriaâ€Upgraded Boron Nitride. Chemistry - an Asian Journal, 2022, 17, .	1.7	6
230	Insight on the anti-poisoning mechanism of <i>in situ</i> coupled sulfate over iron oxide catalysts in NO _{<i>x</i>} reduction. Catalysis Science and Technology, 2022, 12, 4020-4031.	2.1	6
231	Buckypaper of polyvinyl chloride/ <i>p</i> â€phenylenediamine modified graphite and PVC/graphite <i>via</i> resin infiltration technique. Polymer Composites, 2018, 39, 4176-4187.	2.3	5
232	Direct visualization of local deformations in suspended few-layer graphene membranes by coupled in situ atomic force and scanning electron microscopy. Applied Physics Letters, 2021, 118, 103104.	1.5	3
233	Hydrothermal Synthesis of Lithium Titanate as Anode Materials for Lithium-Ion Batteries and its Performance at Different Charging and Discharging Mode. Advanced Materials Research, 2012, 557-559, 1214-1217.	0.3	2
234	Template/surfactant free and UV light irradiation assisted fabrication of Mn-Co oxides composite nanorings: Structure and synthesis mechanism. Progress in Natural Science: Materials International, 2019, 29, 163-169.	1.8	2

#	Article	IF	CITATIONS
235	Revealing the Promotion Effects of Nb on Alkali Resistance of FeVO ₄ /TiO ₂ Catalysts for NO _x Reduction. ChemCatChem, 2022, 14, .	1.8	2
236	Chemical treatment of carbon nanotubes as electrodes in electrochemical double-layer capacitors. Journal of Shanghai University, 2005, 9, 557-560.	0.1	0